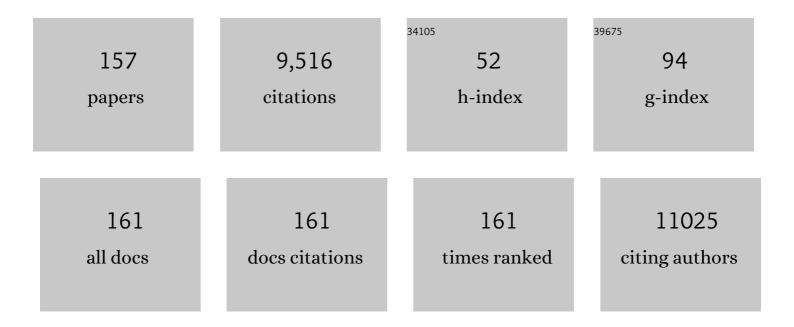
## Angus I Kirkland

List of Publications by Year in descending order

Source: https://exaly.com/author-pdf/1470026/publications.pdf Version: 2024-02-01



ANCUS | KIDKLAND

#	Article	IF	CITATIONS
1	General synthesis and definitive structural identification of MN4C4 single-atom catalysts with tunable electrocatalytic activities. Nature Catalysis, 2018, 1, 63-72.	34.4	1,476
2	A fundamental look at electrocatalytic sulfur reduction reaction. Nature Catalysis, 2020, 3, 762-770.	34.4	455
3	Discrete Atom Imaging of One-Dimensional Crystals Formed Within Single-Walled Carbon Nanotubes. Science, 2000, 289, 1324-1326.	12.6	407
4	Dislocation-Driven Deformations in Graphene. Science, 2012, 337, 209-212.	12.6	332
5	Spatial control of defect creation in graphene at the nanoscale. Nature Communications, 2012, 3, 1144.	12.8	305
6	Nanogold: A Quantitative Phase Map. ACS Nano, 2009, 3, 1431-1436.	14.6	238
7	Dynamics of Single Fe Atoms in Graphene Vacancies. Nano Letters, 2013, 13, 1468-1475.	9.1	228
8	Atomic Structure and Dynamics of Metal Dopant Pairs in Graphene. Nano Letters, 2014, 14, 3766-3772.	9.1	219
9	Integral atomic layer architectures of 1D crystals inserted into single walled carbon nanotubes. Chemical Communications, 2002, , 1319-1332.	4.1	208
10	Transforming carbon dioxide into jet fuel using an organic combustion-synthesized Fe-Mn-K catalyst. Nature Communications, 2020, 11, 6395.	12.8	161
11	An encapsulated helical one-dimensional cobalt iodide nanostructure. Nature Materials, 2003, 2, 788-791.	27.5	156
12	A new method for the determination of the wave aberration function for high resolution TEM. Ultramicroscopy, 2002, 92, 89-109.	1.9	131
13	Structural Reconstruction of the Graphene Monovacancy. ACS Nano, 2013, 7, 4495-4502.	14.6	131
14	Influence of Shell Thickness and Surface Passivation on PbS/CdS Core/Shell Colloidal Quantum Dot Solar Cells. Chemistry of Materials, 2014, 26, 4004-4013.	6.7	129
15	Atomic Structure and Dynamics of Single Platinum Atom Interactions with Monolayer MoS <sub>2</sub> . ACS Nano, 2017, 11, 3392-3403.	14.6	126
16	Synthesis and Structural Characterization of Branched Palladium Nanostructures. Advanced Materials, 2009, 21, 2288-2293.	21.0	124
17	Aberration-Corrected Imaging of Active Sites on Industrial Catalyst Nanoparticles. Angewandte Chemie - International Edition, 2007, 46, 3683-3685.	13.8	117
18	Characterisation of the signal and noise transfer of CCD cameras for electron detection. Microscopy Research and Technique, 2000, 49, 269-280.	2.2	110

#	Article	IF	CITATIONS
19	Atomic Imaging of Phase Transitions and Morphology Transformations in Nanocrystals. Advanced Materials, 2009, 21, 4992-4995.	21.0	104
20	Gold–Palladium Core–Shell Nanocrystals with Size and Shape Control Optimized for Catalytic Performance. Angewandte Chemie - International Edition, 2013, 52, 1477-1480.	13.8	104
21	Structural Characterization of Atomically Regulated Nanocrystals Formed within Single-Walled Carbon Nanotubes Using Electron Microscopy. Accounts of Chemical Research, 2002, 35, 1054-1062.	15.6	103
22	Atomic Structure and Spectroscopy of Single Metal (Cr, V) Substitutional Dopants in Monolayer MoS <sub>2</sub> . ACS Nano, 2016, 10, 10227-10236.	14.6	96
23	Confocal operation of a transmission electron microscope with two aberration correctors. Applied Physics Letters, 2006, 89, 124105.	3.3	92
24	A versatile double aberration-corrected, energy filtered HREM/STEM for materials science. Ultramicroscopy, 2005, 103, 7-15.	1.9	89
25	Materials Advances through Aberration-Corrected Electron Microscopy. MRS Bulletin, 2006, 31, 36-43.	3.5	89
26	Electron ptychographic microscopy for three-dimensional imaging. Nature Communications, 2017, 8, 163.	12.8	89
27	The effects of electron and photon scattering on signal and noise transfer properties of scintillators in CCD cameras used for electron detection. Ultramicroscopy, 1998, 75, 23-33.	1.9	87
28	Crystallization of 2H and 4H PbI2in Carbon Nanotubes of Varying Diameters and Morphologies. Chemistry of Materials, 2006, 18, 2059-2069.	6.7	86
29	Structural changes induced in nanocrystals of binary compounds confined within single walled carbon nanotubes: a brief review. Inorganica Chimica Acta, 2002, 330, 1-12.	2.4	85
30	A Morphology-Selective Copper Organosol. Angewandte Chemie International Edition in English, 1988, 27, 1530-1533.	4.4	84
31	Correlation of Structural and Electronic Properties in a New Low-Dimensional Form of Mercury Telluride. Physical Review Letters, 2006, 96, 215501.	7.8	78
32	Characterisation of the Medipix3 detector for 60 and 80 keV electrons. Ultramicroscopy, 2017, 182, 44-53.	1.9	77
33	Atomic Structure of Graphene Subnanometer Pores. ACS Nano, 2015, 9, 11599-11607.	14.6	75
34	Resolution extension and exit wave reconstruction in complex HREM. Ultramicroscopy, 2004, 98, 99-114.	1.9	72
35	Low-dose phase retrieval of biological specimens using cryo-electron ptychography. Nature Communications, 2020, 11, 2773.	12.8	72
36	"Indirect―High-Resolution Transmission Electron Microscopy: Aberration Measurement and Wavefunction Reconstruction. Microscopy and Microanalysis, 2004, 10, 401-413.	0.4	71

#	Article	IF	CITATIONS
37	Entrapped Single Tungstate Site in Zeolite for Cooperative Catalysis of Olefin Metathesis with BrÃ,nsted Acid Site. Journal of the American Chemical Society, 2018, 140, 6661-6667.	13.7	71
38	Atomically Flat Zigzag Edges in Monolayer MoS <sub>2</sub> by Thermal Annealing. Nano Letters, 2017, 17, 5502-5507.	9.1	70
39	Stability and Dynamics of the Tetravacancy in Graphene. Nano Letters, 2014, 14, 1634-1642.	9.1	68
40	Temperature Dependence of the Reconstruction of Zigzag Edges in Graphene. ACS Nano, 2015, 9, 4786-4795.	14.6	68
41	A new method for the determination of the wave aberration function for high-resolution TEM Ultramicroscopy, 2004, 99, 115-123.	1.9	63
42	Atomic-Scale Detection of Organic Molecules Coupled to Single-Walled Carbon Nanotubes. Journal of the American Chemical Society, 2007, 129, 10966-10967.	13.7	63
43	Molecular nitrogen promotes catalytic hydrodeoxygenation. Nature Catalysis, 2019, 2, 1078-1087.	34.4	63
44	Atomic electrostatic maps of 1D channels in 2D semiconductors using 4D scanning transmission electron microscopy. Nature Communications, 2019, 10, 1127.	12.8	62
45	Resolving strain in carbon nanotubes at the atomic level. Nature Materials, 2011, 10, 958-962.	27.5	61
46	Three-dimensional imaging in double aberration-corrected scanning confocal electron microscopy, Part I:. Ultramicroscopy, 2008, 108, 1558-1566.	1.9	60
47	Atomic Structure of ABC Rhombohedral Stacked Trilayer Graphene. ACS Nano, 2012, 6, 5680-5686.	14.6	59
48	The Morphology and Microstructure of Colloidal Silver and Gold. Angewandte Chemie International Edition in English, 1987, 26, 676-678.	4.4	58
49	On the importance of fifth-order spherical aberration for a fully corrected electron microscope. Ultramicroscopy, 2006, 106, 301-306.	1.9	57
50	Transformations of gold nanoparticles investigated using variable temperature high-resolution transmission electron microscopy. Ultramicroscopy, 2010, 110, 506-516.	1.9	57
51	Atomic structure and formation mechanism of sub-nanometer pores in 2D monolayer MoS <sub>2</sub> . Nanoscale, 2017, 9, 6417-6426.	5.6	54
52	Ultralong 1D Vacancy Channels for Rapid Atomic Migration during 2D Void Formation in Monolayer MoS <sub>2</sub> . ACS Nano, 2018, 12, 7721-7730.	14.6	54
53	Multiple beam tilt microscopy for super resolved imaging. Journal of Electron Microscopy, 1997, 46, 11-22.	0.9	51
54	Direct Imaging of the Structure, Relaxation, and Sterically Constrained Motion of Encapsulated Tungsten Polyoxometalate Lindqvist Ions within Carbon Nanotubes. ACS Nano, 2008, 2, 966-976.	14.6	50

Angus I Kirkland

#	Article	IF	CITATIONS
55	A Study of Commercial Nanoparticulate γâ€Al <sub>2</sub> O <sub>3</sub> Catalyst Supports. ChemCatChem, 2013, 5, 2695-2706.	3.7	50
56	Three-dimensional imaging in double aberration-corrected scanning confocal electron microscopy, Part II: Inelastic scattering. Ultramicroscopy, 2008, 108, 1567-1578.	1.9	47
57	Low-dose aberration corrected cryo-electron microscopy of organic specimens. Ultramicroscopy, 2008, 108, 1636-1644.	1.9	46
58	Nanoscale Energy-Filtered Scanning Confocal Electron Microscopy Using a Double-Aberration-Corrected Transmission Electron Microscope. Physical Review Letters, 2010, 104, 200801.	7.8	46
59	Deterministic electron ptychography at atomic resolution. Physical Review B, 2014, 89, .	3.2	46
60	The development of a 200kV monochromated field emission electron source. Ultramicroscopy, 2014, 140, 37-43.	1.9	46
61	The Role of the Bridging Atom in Stabilizing Odd Numbered Graphene Vacancies. Nano Letters, 2014, 14, 3972-3980.	9.1	44
62	Atomic Resolution Defocused Electron Ptychography at Low Dose with a Fast, Direct Electron Detector. Scientific Reports, 2019, 9, 3919.	3.3	44
63	Detectors—The ongoing revolution in scanning transmission electron microscopy and why this important to material characterization. APL Materials, 2020, 8, .	5.1	44
64	Assessing the precision of strain measurements using electron backscatter diffraction – part 1: Detector assessment. Ultramicroscopy, 2013, 135, 126-135.	1.9	43
65	Aberration measurement using the Ronchigram contrast transfer function. Ultramicroscopy, 2010, 110, 891-898.	1.9	42
66	One-Pot Synthesis of Lithium-Rich Cathode Material with Hierarchical Morphology. Nano Letters, 2016, 16, 7503-7508.	9.1	42
67	A Joint Structural Characterization of Colloidal Platinum by EXAFS and High-Resolution Electron Microscopy. Angewandte Chemie International Edition in English, 1989, 28, 590-593.	4.4	41
68	A composite method for the determination of the chirality of single walled carbon nanotubes. Journal of Microscopy, 2003, 212, 152-157.	1.8	39
69	Bond Length and Charge Density Variations within Extended Arm Chair Defects in Graphene. ACS Nano, 2013, 7, 9860-9866.	14.6	38
70	Controlled formation of closed-edge nanopores in graphene. Nanoscale, 2015, 7, 11602-11610.	5.6	38
71	Inflating Graphene with Atomic Scale Blisters. Nano Letters, 2014, 14, 908-914.	9.1	37
72	Partial Dislocations in Graphene and Their Atomic Level Migration Dynamics. Nano Letters, 2015, 15, 5950-5955.	9.1	37

#	Article	IF	CITATIONS
73	Electron Ptychographic Diffractive Imaging of Boron Atoms in LaB6 Crystals. Scientific Reports, 2017, 7, 2857.	3.3	37
74	Oleylamine Aging of PtNi Nanoparticles Giving Enhanced Functionality for the Oxygen Reduction Reaction. Nano Letters, 2021, 21, 3989-3996.	9.1	37
75	Structural investigation of MoS2core–shell nanoparticles formed by an arc discharge in water. Nanotechnology, 2003, 14, 913-917.	2.6	36
76	Thermally Induced Dynamics of Dislocations in Graphene at Atomic Resolution. ACS Nano, 2015, 9, 10066-10075.	14.6	36
77	Simultaneous Identification of Low and High Atomic Number Atoms in Monolayer 2D Materials Using 4D Scanning Transmission Electron Microscopy. Nano Letters, 2019, 19, 6482-6491.	9.1	36
78	Formation and Healing of Defects in Atomically Thin GaSe and InSe. ACS Nano, 2019, 13, 5112-5123.	14.6	35
79	Phase reconstruction using fast binary 4D STEM data. Applied Physics Letters, 2020, 116, .	3.3	34
80	Experimental evaluation of a spherical aberration-corrected TEM and STEM. Microscopy (Oxford,) Tj ETQq0 0 0 r	gBT /Overl	ock310 Tf 50
81	Controlled Radiation Damage and Edge Structures in Boron Nitride Membranes. ACS Nano, 2011, 5, 3977-3986.	14.6	33
82	Combining Theory and Experiment in Determining the Surface Chemistry of Nanocrystals. Chemistry of Materials, 2008, 20, 5460-5463.	6.7	30
83	Electron nanodiffraction using sharply focused parallel probes. Applied Physics Letters, 2007, 90, 151104.	3.3	28
84	Contrast transfer and noise considerations in focused-probe electron ptychography. Ultramicroscopy, 2021, 221, 113189.	1.9	28
85	Structure and growth of colloidal metal particles. Journal of Chemical Physics, 1989, 91, 603-611.	3.0	27
86	Assessing the precision of strain measurements using electron backscatter diffraction – Part 2: Experimental demonstration. Ultramicroscopy, 2013, 135, 136-141.	1.9	27
87	Hollow Electron Ptychographic Diffractive Imaging. Physical Review Letters, 2018, 121, 146101.	7.8	27
88	Atomic Structure Imaging Beyond Conventional Resolution Limits in the Transmission Electron Microscope. Physical Review Letters, 2009, 103, 126101.	7.8	26
<u> </u>	Local Measurement and Computational Refinement of Aberrations for HRTEM. Microscopy and	0.4 —	94 -

90Structure Determination of Atomically Controlled Crystal Architectures Grown within Single Wall<br/>Carbon Nanotubes. Microscopy and Microanalysis, 2005, 11, 401-409.0.423

Microanalysis, 2006, 12, 461-468.

#	Article	IF	CITATIONS
91	Structural characterization of interfaces in epitaxial Fe/MgO/Fe magnetic tunnel junctions by transmission electron microscopy. Physical Review B, 2010, 82, .	3.2	22
92	Cation segregation in Nb16W18O94 using high angle annular dark field scanning transmission electron microscopy and image processing. Journal of Microscopy, 2002, 206, 1-6.	1.8	21
93	Imaging and Characterization of Molecules and One-Dimensional Crystals Formed within Carbon Nanotubes. MRS Bulletin, 2004, 29, 265-271.	3.5	21
94	Imaging the Active Surfaces of Cerium Dioxide Nanoparticles. ChemPhysChem, 2011, 12, 2397-2399.	2.1	20
95	Impurity induced non-bulk stacking in chemically exfoliated h-BN nanosheets. Nanoscale, 2013, 5, 2290.	5.6	20
96	Calculations of spherical aberration-corrected imaging behaviour. Journal of Electron Microscopy, 2003, 52, 359-364.	0.9	18
97	Observation of octahedral cation coordination on the {111} surfaces of iron oxide nanoparticles. Applied Physics Letters, 2006, 88, 093124.	3.3	18
98	Temperature dependence of atomic vibrations in mono-layer graphene. Journal of Applied Physics, 2015, 118, .	2.5	18
99	Imaging Three-Dimensional Elemental Inhomogeneity in Pt–Ni Nanoparticles Using Spectroscopic Single Particle Reconstruction. Nano Letters, 2019, 19, 732-738.	9.1	18
100	Optimal tilt magnitude determination for aberration-corrected super resolution exit wave function reconstruction. Philosophical Transactions Series A, Mathematical, Physical, and Engineering Sciences, 2009, 367, 3755-3771.	3.4	17
101	Effect of amorphous layers on the interpretation of restored exit waves. Ultramicroscopy, 2009, 109, 237-246.	1.9	16
102	Comparisons of Linear and Nonlinear Image Restoration. Microscopy and Microanalysis, 2006, 12, 469-475.	0.4	15
103	High-Resolution TEM and the Application of Direct and Indirect Aberration Correction. Microscopy and Microanalysis, 2008, 14, 60-67.	0.4	15
104	Calculations of HREM image intensity using Monte Carlo integration. Ultramicroscopy, 2005, 104, 271-280.	1.9	14
105	Structural correlation of band-gap modifications induced in mercury telluride by dimensional constraint in single walled carbon nanotubes. Physica Status Solidi (B): Basic Research, 2006, 243, 3257-3262.	1.5	14
106	Recording low and high spatial frequencies in exit wave reconstructions. Ultramicroscopy, 2013, 133, 26-34.	1.9	14
107	Characterization of grain boundary disconnections in SrTiO3 Part II: the influence of superimposed disconnections on image analysis. Journal of Materials Science, 2019, 54, 3710-3725.	3.7	12
108	Quantifying the performance of a hybrid pixel detector with GaAs:Cr sensor for transmission electron microscopy. Ultramicroscopy, 2021, 227, 113298.	1.9	12

#	Article	IF	CITATIONS
109	Transmission electron microscopy without aberrations: Applications to materials science. Current Applied Physics, 2008, 8, 425-428.	2.4	11
110	Lal <sub>2</sub> @(18,3)SWNT: The Unprecedented Structure of a Lal <sub>2</sub> "Crystal,― Encapsulated within a Single-Walled Carbon Nanotube. Microscopy and Microanalysis, 2005, 11, 421-430.	0.4	10
111	Snapshot 3D Electron Imaging of Structural Dynamics. Scientific Reports, 2017, 7, 10839.	3.3	10
112	HREM of the {111} surfaces of iron oxide nanoparticles. Micron, 2006, 37, 389-395.	2.2	9
113	Dose-dependent high-resolution electron ptychography. Journal of Applied Physics, 2016, 119, .	2.5	9
114	Platinum supported on pristine and nitrogen-doped bowl-like broken hollow carbon spheres as oxygen reduction reaction catalysts. Journal of Applied Electrochemistry, 2021, 51, 991-1008.	2.9	9
115	Ultrahigh resolution imaging of local structural distortions in intergrowth tungsten bronzes. Ultramicroscopy, 2007, 107, 501-506.	1.9	8
116	Exit wave reconstruction from focal series of HRTEM images, single crystal XRD and total energy studies on Sb <sub><i>x</i></sub> WO <sub>3+<i>y</i></sub> ( <i>x</i> â^1⁄4 0.11). Zeitschrift Fur Kristallographie - Crystalline Materials, 2012, 227, 341-349.	0.8	8
117	Exceeding Conventional Resolution Limits in High-Resolution Transmission Electron Microscopy Using Tilted Illumination and Exit-Wave Restoration. Microscopy and Microanalysis, 2010, 16, 409-415.	0.4	7
118	Trainable segmentation for transmission electron microscope images of inorganic nanoparticles. Journal of Microscopy, 2022, 288, 169-184.	1.8	7
119	Direct and Indirect Electron Microscopy of Encapsulated Nanocrystals. Topics in Catalysis, 2002, 21, 139-154.	2.8	6
120	DFT calculations of KI crystals formed within single-walled carbon nanotubes. Chemical Physics Letters, 2008, 466, 76-78.	2.6	6
121	Low-Dose Scanning Electron Diffraction Microscopy of Mechanochemically Nanostructured Pharmaceuticals. Microscopy and Microanalysis, 2019, 25, 1746-1747.	0.4	6
122	The characterization of sub-nanometer scale structures within single walled carbon nanotubes. AIP Conference Proceedings, 2001, , .	0.4	5
123	Structural characterization of the n = 5 layered perovskite neodymium titanate using high-resolution transmission electron microscopy and image reconstruction. Acta Crystallographica Section B: Structural Science, 2003, 59, 449-455.	1.8	5
124	Aberration measurement of the probe-forming system of an electron microscope using two-dimensional materials. Ultramicroscopy, 2017, 182, 195-204.	1.9	5
125	Low Dose Defocused Probe Electron Ptychography Using a Fast Direct Electron Detector. Microscopy and Microanalysis, 2018, 24, 186-187.	0.4	5
126	Parakeet: a digital twin software pipeline to assess the impact of experimental parameters on tomographic reconstructions for cryo-electron tomography. Open Biology, 2021, 11, 210160.	3.6	5

Angus I Kirkland

#	Article	IF	CITATIONS
127	Exit wave reconstruction of radiation-sensitive materials from low-dose data. Journal of Physics: Conference Series, 2014, 522, 012052.	0.4	4
128	Atomic Resolution Transmission Electron Microscopy. Springer Handbooks, 2019, , 3-47.	0.6	4
129	The application of spherical aberration correction and focal series restoration to high-resolution images of platinum nanocatalyst particles. Journal of Physics: Conference Series, 2006, 26, 25-28.	0.4	3
130	Aberration corrected TEM: current status and future prospects. Journal of Physics: Conference Series, 2008, 126, 012034.	0.4	3
131	High Resolution ExitWave Restoration. Nanostructure Science and Technology, 2012, , 41-72.	0.1	3
132	Fast and Low-dose Electron Ptychography. Microscopy and Microanalysis, 2018, 24, 224-225.	0.4	3
133	Contrast Transfer and Noise Minimization in Electron Ptychography. Microscopy and Microanalysis, 2019, 25, 64-65.	0.4	3
134	Three-dimensional Electron Ptychography of Catalyst Nanoparticles using Combined HAADF STEM and Atom Counting. Microscopy and Microanalysis, 2019, 25, 8-9.	0.4	3
135	The Crystallography of Metal Halides formed within Single Walled Carbon Nanotubes. Materials Research Society Symposia Proceedings, 2000, 633, 14311.	0.1	2
136	HREM of metallized {111} iron oxide nanoparticle surfaces. Journal of Physics: Conference Series, 2006, 26, 191-194.	0.4	2
137	Atomic Resolution Transmission Electron Microscopy. , 2007, , 3-64.		2
138	Toward electron exit wave tomography of amorphous materials at atomic resolution. Journal of Alloys and Compounds, 2012, 536, S94-S98.	5.5	2
139	Observing Structural Dynamics and Measuring Chemical Kinetics in Low Dimensional Materials Using High Speed Imaging. Microscopy and Microanalysis, 2019, 25, 1682-1683.	0.4	2
140	3D Electron Ptychography. Microscopy and Microanalysis, 2019, 25, 1802-1803.	0.4	2
141	Finding phase information in the darkness. Journal of Physics: Conference Series, 2010, 241, 012013.	0.4	1
142	Toward 3D structural information from quantitative electron exit wave analysis. Journal of Physics: Conference Series, 2012, 371, 012057.	0.4	1
143	Imaging Structure and Magnetisation in New Ways Using 4D STEM. Microscopy and Microanalysis, 2018, 24, 180-181.	0.4	1
144	Electron ptychography using an ultrafast direct electron detector. Microscopy and Microanalysis, 2019, 25, 20-21.	0.4	1

#	Article	IF	CITATIONS
145	Ptychographic Single Particle Analysis for Biological Science. Microscopy and Microanalysis, 2021, 27, 190-192.	0.4	1
146	Band-Gap Modification Induced in HgTe by Dimensional Constraint in Carbon Nanotubes: Effect of Nanotube Diameter on Microstructure. Springer Proceedings in Physics, 2008, , 213-216.	0.2	1
147	Aberration-corrected HREM/STEM for semiconductor research. , 2005, , 177-182.		1
148	Aberration corrected tilt series restoration. Journal of Physics: Conference Series, 2008, 126, 012042.	0.4	0
149	Inside Cover: Imaging the Active Surfaces of Cerium Dioxide Nanoparticles (ChemPhysChem 13/2011). ChemPhysChem, 2011, 12, 2358-2358.	2.1	0
150	Electron Ptychography: From 2D to 3D Reconstructions. Microscopy and Microanalysis, 2017, 23, 346-347.	0.4	0
151	Phase Retrieval Quantitative Comparison Between Tilt-series Imaging in TEM and Position-resolved Coherent Diffractive Imaging in STEM. Microscopy and Microanalysis, 2017, 23, 470-471.	0.4	0
152	Using Advanced STEM Techniques to Unravel Key Issues in the Development of Next-Generation Nanostructures for Energy Storage. Microscopy and Microanalysis, 2017, 23, 1698-1699.	0.4	0
153	STEM and Elemental Analysis by EDS and EELS for Two-dimensional Atomic Structure Containing Au and Cu. Microscopy and Microanalysis, 2019, 25, 1776-1777.	0.4	0
154	Three-Dimensional Imaging of Nanoparticle Chemistry Using Spectroscopic Single Particle Reconstruction. Microscopy and Microanalysis, 2019, 25, 400-401.	0.4	0
155	Low Dose Electron Ptychography for Cryo-biological Imaging. Microscopy and Microanalysis, 2020, 26, 1488-1490.	0.4	0
156	A 3D map of atoms in 2D materials. Nature Materials, 2020, 19, 827-828.	27.5	0
157	Elmar Zeitler (1927–2020). Ultramicroscopy, 2021, 229, 113366.	1.9	Ο